A study on some basic features of inertial oscillations and near-inertial internal waves

Shengli Chen, Daoyi Chen, Jiuxing Xing

Shenzhen Key Laboratory for Coastal Ocean Dynamic and Environment, Graduate School at Shenzhen, Tsinghua University, Shenzhen 518055, China.

Correspondence to: Jiuxing Xing (jxx2012@sz.tsinghua.edu.cn)

23   **Abstract**

24   Some basic features of inertial oscillations and near-inertial internal waves are investigated by simulating

25   a two-dimensional (x-z) rectangular basin (300 km $\times$60 m) driven by a wind pulse. For the homogeneous

26   case, near-inertial motions are pure inertial oscillations. The inertial oscillation shows typical opposite

27   currents between surface and lower layers, which is formed by the feedback between barotropic waves

28   and inertial currents. For the stratified case, near-inertial internal waves are generated at land boundaries

29   and propagate offshore with higher frequencies, which induce tilting of velocity contours in the

30   thermocline. The inertial oscillation is uniform across the whole basin, except near the coastal boundaries

31   (~20 km) where it quickly declines to zero. This boundary effect is related to great enhancement of

32   nonlinear terms, especially the vertical nonlinear term ($w\partial\mathbf{u}/\partial z$). With the inclusion of near-inertial

33   internal waves, the total near-inertial energy has a slight change, with occurrence of a small peak at ~50

34   km, which is similar to previous researches. We conclude that, for this distribution of near-inertial energy,

35   the boundary effect for inertial oscillations is primary, and the near-inertial internal wave plays a

36   secondary role. Homogeneous cases with various water depths (50 m, 40 m, 30 m, 20 m) are also

37   simulated. It is found near-inertial energy monotonously declines with decreasing water depth, because

38   more energy of the initial wind-driven currents is transferred to seiches by barotropic waves. For the case

39   of 20 m, the seiches energy even slightly exceeds the near-inertial energy. We suppose this is an important

40   reason why near-inertial motions are weak and hardly observed in coastal regions.

41

42   **Keywords:** inertial oscillations, near-inertial internal waves, near-inertial energy

43

44

45

46

47

48

1. Introduction

Near-inertial motion has been observed and reported in many seas (e.g. Alford et al., 2016; Webster, 1968). It is mainly generated by changing winds at the sea surface (Pollard and Millard, 1970; Chen et al., 2015b). The passage of a cyclone or a front can induce very strong near-inertial motions(D'Asaro, 1985), which can last for 1-2 weeks and reach a maximum velocity magnitude of 0.5-1.0 m/s (Chen et al., 2015a; Zheng et al., 2006; Sun et al., 2011). In deep seas, the near-inertial internal wave propagates downwards to transfer energy to depth (Leaman and Sanford, 1975; Fu, 1981; Gill, 1984; Alford et al., 2012). The strong vertical shear of near-inertial currents may play an important role in inducing mixing across the thermocline (Price, 1981; Burchard and Rippeth, 2009; Chen et al., 2016).

In shelf seas, near-inertial motions exhibit a two-layer structure, with an opposite phase between currents in the surface and lower layers (Malone, 1968; Millot and Crepon, 1981; MacKinnon and Gregg, 2005). By solving a two-layer analytic model using the Laplace transform, Pettigrew (1981) found this 'baroclinic' structure can be formed by inertial oscillations without inclusion of near-inertial internal waves. Due to similar vertical structure and frequencies, inertial oscillations and near-inertial internal waves are hardly separable, and could easily be mistakenly recognized as each other.

In shelf seas, the near-inertial energy increases gradually offshore, and reaches a maximum near the shelf break, found both in observations (Chen et al., 1996) and model simulations (Xing et al., 2004; Nicholls et al., 2012). Chen and Xie (1997) reproduced this cross-shelf variation both in linear and nonlinear simulations, and attribute it to large values of the cross-shelf gradient of surface elevation and the vertical gradient of Reynolds stress near the shelf break. By using the analytic model of Pettigrew (1981), Shearman (2005) argued that the cross-shelf variation is controlled by baroclinic waves which emanate from the coast to introduce nullifying effects on the near-inertial energy near shore. Kundu et al. (1983) found a coastal inhibition of near-inertial energy within the Rossby radius from the coast, which is attributed to leaking of near-inertial energy downward and offshore. As many factors seems to work, the mechanism controlling the cross-shelf variation of near-inertial energy is not clear.

In this paper, simple two-dimensional simulations are used to investigate some basic features of near-inertial motions. Cases with and without vertical stratification are simulated to examine properties and differences between inertial oscillations and near-inertial internal waves. The horizontal distribution of

77 near-inertial energy is discussed in detail. Also cases with various water depths are simulated to

78 investigate the dependence of near-inertial motions on the water depth.

2. Model Settings

80 The simulated region is a two-dimensional shallow rectangular basin (300 km $\times$ 60 m). Numerical

81 simulations are done by the MIT general circulation model (MITgcm) (Marshall et al., 1997), which

82 discretizes the primitive equations and can be designed to model a wide range of phenomena. There are

83 1500 grid points in the horizontal (Δx =200 m) and 60 grid points in vertical (Δz =1 m). The water

84 depth is uniform, with east and west sides being land boundaries. The vertical and horizontal eddy

85 viscosities are assumed constant as 5×10^{-4} m^2/s and 10 m^2/s, respectively. The Coriolis parameter is 5×10^{-5} s^{-1} (at a latitude of 20.11 °N). The bottom boundary is no-slip. The model is forced by a spatially uniform

87 wind which is kept westward and increases from 0 to 0.73 N/m^2 (corresponding to a wind speed of 20

88 m/s) for the first three hours and then suddenly stops. The model runs for 200 hours in total, with a time

89 step of 4 seconds. The first case is homogeneous, while the second one has a stratification of two-layer

90 structure initially. For the stratified case, the temperature is 20℃ in the upper layer (-30 m<z<0), and

91 15℃ in the lower layer (-60 m<z<-30 m). The salinity is constant, and the density is linearly determined

92 by the temperature, with an expansion coefficient of 2×10^{-4} ℃$^{-1}$. The barotropic and baroclinic radii are

93 485 km and 8 km, respectively.

3. Inertial oscillation

95 The first case is without the presence of vertical stratification. Thus the near-inertial internal wave is

96 absent, and the near-inertial motion is a pure inertial oscillation.

3.1 Vertical structures

98 The model simulated velocities (Fig. 1) vary near the inertial period (34.9 hours). Spectra of velocities

99 (not shown) indicate maximum peaks located exactly at the inertial period. The spectra of u also have a

100 smaller peak at the period of the first mode seiche (6.9 hours). As this simulation is two-dimensional,

101 i.e., the gradient along *y*-axis is zero, the *u*/*v* of seiche have a value of ω_n/f (equals 5 for the first mode

102 seiche). Thus there is little energy of seiche in *v* which shows clearly regular variation at the inertial

103 frequency.

104 In the vertical direction, currents display a two-layer structure, with their phase being opposite between

105 surface and lower layers. They are maximum at the surface, and have a weaker maximum in the lower

106 layer (~40 m), with a minimum at the depth of ~20 m. The velocity gradually diminishes to zero at the

107 bottom due to the bottom friction. This is the typical vertical structure of shelf-sea inertial oscillations,

108 which have been frequently observed (Shearman, 2005; MacKinnon and Gregg, 2005). In practice, this

109 vertical distribution can be modified due to presence of other processes, such as the surface maximum

110 being pushed down to the subsurface (e.g. Chen et al., 2015a). Note that without stratification in this

111 simulation the near-inertial internal wave is absent. However, this two-layer structure of inertial

112 oscillations looks 'baroclinic', which makes it easy to be mistakenly attributed to the near-inertial internal

113 wave (Pettigrew, 1981).

114 It is interesting that currents of non-baroclinic inertial oscillations reverse between the surface and lower

115 layers. This is usually due to the presence of the coast, which requires the normal-to-coast transport to

116 be zero, thus currents in upper and lower layers compensate each other (e.g., Millot and Crepon, 1981;

117 Chen et al., 1996). However, it remains unclear how this vertical structure is established step by step.

118 As the westward wind blows for the first three hours, the initial inertial current is also westward and only

119 exists in the very surface layer (Fig. 2). In the lower layer there is no movement initially. Thus a westward

120 transport is produced, which generates a rise (in the west) and fall (in the east) of elevation near land

121 boundaries. The elevation slope behaves in a form of barotropic wave which propagates offshore at a

122 large speed (87 km/h). The current driven by the barotropic wave is eastward, and uniform vertically.

123 Therefore, with the arrival of the barotropic wave the westward current in the surface is reduced, and the

124 eastward movement in the lower layer commences (Fig. 2). After the passage of the first two barotropic

125 waves (originated from both sides), currents in the lower layer have reached a relatively large value,

126 while currents in the surface layer have largely decreased (Fig. 3a). Accordingly, the depth-integrated

127 transport diminishes a lot. This is a feedback between inertial currents and barotropic waves. If only the

128 depth-integrated transport of currents exist, barotropic waves will be generated, which reduce the surface

129 currents but increase the lower layer currents, and thus reduces the current transport. It will end up with

130 inertial currents in the surface and lower layers having opposite directions and comparable amplitudes.

131 As seen from Fig. 1b, the typical vertical structure of inertial currents is established within the first inertial

132 period.

133 **3.2 Horizontal distributions of inertial energy**

134 The inertial velocities are almost entirely the same across the basin (Fig. 4), except near the boundary.

135 This indicates that inertial oscillations have a coherence scale of almost the basin width. This is because

136 in our simulation the wind force is spatially uniform, and the bottom is flat. The inertial velocities in the

137 lower layer have slightly more variation across the basin than those in the surface layer, because inertial

138 velocities in the lower layer depend on the propagation of barotropic waves as discussed in 3.1, while

139 the surface inertial currents are driven by spatially uniform wind. In shelf sea regions, the wind forcing

140 is usually coherent as the synoptic scale is much larger, however, the topography that is mostly not flat

141 could generate barotropic waves at various places, and thus significantly decrease coherence of inertial

142 currents in the lower layer.

143 The spectra of velocities in the inertial band are almost uniform except near the boundaries (Fig. 5),

144 consistent with the velocities. Near the boundaries, the inertial energy declines gradually to zero from

145 x=~20 km to the land. The east side has slightly greater inertial energy and a slight wider boundary layer

146 compared to the west side.

147 We calculate the nonlinear and inertial terms in the momentum equation and find that nonlinear terms

148 are of significantly high values initially within 2 km away from the land boundary (Fig 6bc), where the

149 inertial term is weak (Fig 6a). For the time-averaged values (Fig 6d), the vertical nonlinear term is two

150 times more than the horizontal nonlinear term. The inertial term drops sharply near the boundary, and

151 rises gradually with the distance away from the boundary. At x> 15km, it keeps an almost constant value

152 which is much greater than nonlinear terms. Thus it is concluded that the significant decrease of inertial

153 oscillations near the boundary is due to influence of nonlinear terms, especially the vertical nonlinear

154 term.

155 **4.   Near-inertial internal waves**

156 In addition to inertial oscillations, near-inertial internal waves are usually generated along when the

157 vertical stratification is present. However, due to their close frequencies inertial oscillations and near-

158 inertial internal waves are difficult to be separated. Thus we run a second simulation with the presence

159 of stratification to investigate the differences that near-inertial internal waves introduce.

160 **4.1 Temperature distributions**

161 Fig. 7 shows the evolution of temperature profiles with time. One can see an internal wave packet is

162   generated at the west coast, and then propagates offshore. The wave phase speed is around 1 km/h, close

163   to the theoretical value (1.4 km/h). Before the arrival of internal waves, the temperature at mid-depth

164   diffuses gradually due to vertical diffusion in the model. For a fixed position at x=20 km (Fig. 8), the

165   temperature varies with the inertial period (34.9 hours) and the amplitude of fluctuation declines

166   gradually with time. At x=60 km and x=100 km, the strength of internal waves is much reduced. And

167   wave periods are shorter initially, followed by a gradually increase to the inertial period. At x=140 km,

168   the internal wave becomes as weak as the background disturbance.

169   A spectral analysis of the temperature at mid-depth (z=-30 m) is shown in Fig. 9a. The strongest peak is

170   at near the inertial frequency (0.69 cpd), but only confined to the region close to the boundary (x<40 km).

171   In the region 20km<x<70km, the energy is also large at higher frequencies of 0.8-1.7 cpd. This generally

172   agrees with properties of Poincaré waves. During Rossby adjustment, the waves with higher frequencies

173   propagate offshore at greater group speeds, thus for places further offshore the waves have higher

174   frequencies (Millot and Crepon, 1981). While the wave with a frequency closest to the inertial frequency

175   moves at the slowest group velocity, and it takes a relatively long time to propagate far offshore, thus it

176   is mostly confined to near the boundary. By solving an idealized two-layer model equation, the response

177   of Rossby adjustment can be expressed in form of Bessel functions (Millot and Crepon, 1981; Gill, 1982;

178   Pettigrew, 1981), as in Fig. 9cd showing the spectra of mid-depth elevation. The difference from our case

179   is obvious. The frequency of theoretical near-inertial waves increase gradually with the distance from the

180   coast, while in our case this property is absent. And the theoretical inertial energy has a e-folding scale

181   of 54 km, while in our case the e-folding scale is much smaller (~15 km).

182   **4.2 Velocity distributions**

183   With presence of near-inertial internal waves, the contours of velocities near the thermocline tilt slightly

184   (Fig. 10d), and indicates an upward propagation of phase, thus a downward energy flux. This can also be

185   seen in vertical spirals of velocities (Figs. 10e and 10f). With only inertial oscillations, current vectors

186   mostly point toward two opposite directions (Figs. 10b and 10c). Once the near-inertial wave is included,

187   the current vectors gradually rotate clockwise with depth.

188   The spatial distribution of the near-inertial energy is also slightly changed compared to the case with only

189   inertial oscillations (Fig. 11 and Fig. 5). It is also greatly reduced to zero in the boundary layer (0-20 km)

7

190 like the case without stratification. But at ~50 km away from the boundary the inertial energy reaches a

191 peak. Further away (>100 km) it becomes a constant. This spatial distribution of inertial energy is similar

192 to that observed in shelf seas, with a maximum near the shelf break (Chen et al., 1996; Shearman, 2005).

193 In our case, the boundary layer effect which induces a sharp decrease to zero makes a major contribution,

194 and near-inertial internal waves which bring a small peak further offshore have a secondary influence.

195 **5. Dependence on the water depth**

196 In coastal regions, near-inertial motions are rarely reported. It is speculated that the strong dissipation

197 and bottoms friction in coastal region suppress the development of near-inertial motions. However, Chen

198 (2014) found the water depth is also a sensitive factor, with significant reduction for the case with smaller

199 water depth. Here we will run cases with different water depths and clarify why the near-inertial energy

200 changes with water depth. Homogeneous cases with water depths of 50 m, 40 m, 30 m, 20 m are

201 simulated. The vertical interval for all cases is 1 m. All the other parameters including viscosities are the

202 same as the homogeneous case of 60 m.

203 For each case, the currents are band-pass filtered to obtain near-inertial currents. Then near-inertial

204 kinetic energy can be calculated. As seen in Fig. 12, the near-inertial energy gradually declines with

205 decreasing water depth. In this dynamical system, the other dominant process is the seiches induced by

206 barotropic waves. As the elevation induced by seiches is anti-symmetric in such a basin, the potential

207 energy is little. The kinetic energy of siehces can also be calculated by the band-pass filtered currents.

208 We find the energy of seiches, by contrast, increases gradually with decreasing water depth. For the case

209 of 60 m, the near-inertial energy is much greater than the seiches energy. But for the case of 20 m, the

210 energy of seiches has exceeded the near-inertial energy slightly. The total energy of these two processes

211 almost keeps constant for all cases. For a shallower water depth, the reduction of near-inertial energy

212 equals the increase of seiches energy. The initial current is wind-driven and only distributes in the surface

213 layer. The unbalanced across-shelf flow generates elevation near the land boundary which propagates

214 offshore as barotropic waves and form seiches. Part of the energy goes to form inertial oscillations. For

215 a shallower water depth, the elevation is enlarged, and more energy is transferred to form seiches, thus

216 with weakened near-inertial motions. Therefore, in coastal regions with water depth less than 30m, the

217 near-inertial motion is weak, due to the suppression of barotropic waves.

218   As seen in Section 3.1, inertial oscillations behave in a two-layer structure, with currents in the upper

219   layer in opposite phase with those of lower layer. In terms of kinetic energy, for the case of 60 m (Fig.

220   13), the near-inertial motion is maximized in the very surface, minimized near the depth of 20 m, and

221   then gradually increases with depth to form a much smaller peak at 40 m. Near the bottom, the near-

222   inertial energy gradually reduces to zero due to bottom friction. When we set the bottom boundary

223   condition from nonslip to slip, such a boundary structure vanishes, and near-inertial energy become

224   constant in the lower layer. For other cases of 20 m and 40 m, their vertical profile are almost the same

225   as the 60 m case. The minimum positions are all located at 1/3 of the water depth. This implies the

226   vertical distribution of near-inertial energy is independent of water depth. Note that in our cases, the

227   vertical viscosity is set as a constant value. In practice, the viscosity in the thermocline is usually

228   significantly reduced, thus the minimum position of near-inertial energy is located just below the mixed

229   layer.

230   **6.   Summary and discussion**

231   Idealized simple two-dimensional (x-z) simulations are conducted to examine the response of a shallow

232   closed basin to a wind pulse. The first case is homogeneous, in which the near-inertial motion is a pure

233   inertial oscillation. It has a two-layer structure, with currents in the surface and lower layers being

234   opposite in phase, which has been reported frequently in shelf seas. We find that the inertial current is

235   confined in the surface layer initially. The induced depth-integrated transport generates barotropic waves

236   near the boundaries which propagates quickly offshore. The flow driven by the barotropic wave is

237   independent of depth and opposite to the surface flow. Thus the surface flow is reduced but the flow in

238   the lower layer is increased, as a result the transport diminishes. This feedback between barotropic waves

239   and currents continues and ends up with the depth-integrated transport vanishing, i.e., inertial currents in

240   the upper and lower layers having opposite phases and comparable amplitudes. In our simulation, within

241   just one inertial period the typical structure of inertial currents has been established. By solving a two-

242   layer analytic model using the Laplace transform, Pettigrew (1981) also found the vertical structure of

243   opposite currents associated with inertial oscillations. He argued that the arrival of a barotropic wave for

244   a fixed location cancels half of the inertial oscillation in the surface layer, and initiates an equal and

245   opposite oscillation in the lower layer. However, in our simulation the arrival of the first barotropic wave

246   cannot cancel half of the surface flow. The balanced state of upper and lower flows takes more time to

9

247   reach.

248   The second case is a setup with idealized two-layer stratification, thus near-inertial internal waves are

249   generated. For a fixed position, velocity contours show clear obvious tilting near the thermocline, and

250   velocity vectors display clearly anti-cyclonic spirals with depth. These could be useful clues to examine

251   occurrence of near-inertial internal waves. Near the land boundary the vertical elevation generates

252   fluctuations of thermocline that propagate offshore. The energy of near-inertial internal waves is confined

253   to near the land boundary (x< 40 km). At positions further offshore, the waves have higher frequencies.

254   This is generally consistent with properties of a Rossby adjustment process. However, our simulated

255   results also show evident discrepancies from theoretical values obtained in the classic solutions of Rossby

256   adjustment problem, which are probably attributed to nonlinearity of the model.

257   The inertial oscillation has a very large coherent scale of almost the whole basin scale. It is uniform in

258   both amplitude and phase across the basin, except near the boundary (~20 km offshore). The energy of

259   inertial oscillations declines gradually to zero from x=20 km to the coast. This boundary effect is

260   attributed to influence of nonlinear terms, especially the vertical term ($w\partial \mathbf{u}/\partial z$), which are greatly

261   enhanced near the boundary, and overweighs the inertial term ($f\mathbf{u}$). When near-inertial internal waves

262   are produced in the stratified case, the distribution of total near-inertial energy is modified slightly near

263   the boundary. A small peak appears at ~ 50 km offshore. This is similar to the cross-shelf distribution of

264   near-inertial energy observed in shelf seas (Chen et al., 1996; Shearman, 2005). This energy distribution

265   has been attributed to downward and offshore leakage of near-inertial energy near the coast (Kundu et

266   al., 1983), the variation of elevation and Reynolds stress terms associated with the topography (Chen and

267   Xie, 1997) and the influence of the baroclinic wave (Shearman, 2005; Nicholls et al., 2012). In our

268   simulations, this horizontal distribution of near-inertial energy is primarily controlled by the boundary

269   effect on inertial oscillations, and the near-inertial internal wave has a secondary effect.

270   Homogeneous cases with various water depths (50 m, 40 m, 30 m, and 20 m) are also simulated. The

271   inertial energy is reduced with decreasing water depth, while the energy of seiches, by contrast, is

272   increased. For the case of 20 m, the seiches energy has slightly exceeds the inertial energy. It is interesting

273   that the reduction of inertial energy just equals the increase of seiches energy, which implies more energy

274   of initial wind-driven currents is transferred to the seiches for the shallower cases, and thus less energy

275   goes to the inertial process. This is probably an important reason why near-inertial motions are weak and

276   rarely reported in shallow coastal regions.

277

278

279

286

287

288

289   **References**

290   Alford, M. H., Cronin, M. F., and Klymak, J. M.: Annual Cycle and Depth Penetration of Wind-Generated
291   Near-Inertial Internal Waves at Ocean Station Papa in the Northeast Pacific, Journal of Physical
292   Oceanography, 42, 889-909, 10.1175/jpo-d-11-092.1, 2012.

293   Alford, M. H., MacKinnon, J. A., Simmons, H. L., and Nash, J. D.: Near-Inertial Internal Gravity Waves in
294   the Ocean, Ann Rev Mar Sci, 8, 95-123, 10.1146/annurev-marine-010814-015746, 2016.

295   Burchard, H., and Rippeth, T. P.: Generation of Bulk Shear Spikes in Shallow Stratified Tidal Seas,
296   Journal of Physical Oceanography, 39, 969-985, 10.1175/2008jpo4074.1, 2009.

297   Chen, C., and Xie, L.: A numerical study of wind-induced, near-inertial oscillations over the Texas-
298   Louisiana shelf, Journal of Geophysical Research: Oceans, 102, 15583-15593, 10.1029/97jc00228,
299   1997.

300   Chen, C. S., Reid, R. O., and Nowlin, W. D.: Near-inertial oscillations over the Texas Louisiana shelf, J
301   Geophys Res-Oceans, 101, 3509-3524, 10.1029/95jc03395, 1996.

302   Chen, S.: Study on Several Features of the Near-inertial Motion, PhD, Xiamen University, 107 pp.,
303   2014.

304   Chen, G., Xue, H., Wang, D., and Xie, Q.: Observed near-inertial kinetic energy in the northwestern

11

305   South China Sea, J Geophys Res-Oceans, 118, 4965-4977, 10.1002/jgrc.20371, 2013.

306   Chen, S., Hu, J., and Polton, J. A.: Features of near-inertial motions observed on the northern South

307   China Sea shelf during the passage of two typhoons, Acta Oceanologica Sinica, 34, 38-43,

308   10.1007/s13131-015-0594-y, 2015a.

309   Chen, S., Polton, J. A., Hu, J., and Xing, J.: Local inertial oscillations in the surface ocean generated by

310   time-varying winds, Ocean Dynamics, 65, 1633-1641, 10.1007/s10236-015-0899-6, 2015b.

311   Chen, S., Polton, J. A., Hu, J., and Xing, J.: Thermocline bulk shear analysis in the northern North Sea,

312   Ocean Dynamics, 66, 499-508, 10.1007/s10236-016-0933-3, 2016.

313   D'Asaro, E. A.: The energy flux from the wind to near-inertial motions in the surface mixed layer,

314   Journal of Physical Oceanography, 15, 1043-1059, 1985.

315   Fu, L. L.: Observations and models of inertial waves in the deep ocean, Reviews of Geophysics, 19,

316   141-170, 10.1029/RG019i001p00141, 1981.

317   Gill, A. E.: Atmosphere-ocean dynamics, Academic Press, 662 pp., 1982.

318   Gill, A. E.: On the behavior of internal waves in the wakes of storms, Journal of Physical Oceanography,

319   14, 1129-1151, 10.1175/1520-0485(1984)014<1129:otboiw>2.0.co;2, 1984.

320   Kundu, P. K., Chao, S. Y., and McCreary, J. P.: Transient coastal currents and inertio-gravity waves, Deep-

321   Sea Research Part a-Oceanographic Research Papers, 30, 1059-1082, 10.1016/0198-0149(83)90061-4,

322   1983.

323   Leaman, K. D., and Sanford, T. B.: Vertical energy propagation of inertial waves: a vector spectral

324   analysis of velocity profiles, Journal of Geophysical Research, 80, 1975-1978, 1975.

325   MacKinnon, J. A., and Gregg, M. C.: Near-inertial waves on the New England shelf: The role of evolving

326   stratification, turbulent dissipation, and bottom drag, Journal of Physical Oceanography, 35, 2408-

327   2424, 10.1175/jpo2822.1, 2005.

328   Malone, F. D.: An analysis of current measurements in Lake Michigan, Journal of Geophysical

329   Research, 73, 7065-&, 10.1029/JB073i022p07065, 1968.

330   Marshall, J., Adcroft, A., Hill, C., Perelman, L., and Heisey, C.: A finite-volume, incompressible Navier

331   Stokes model for studies of the ocean on parallel computers, Journal of Geophysical Research: Oceans,

332   102, 5753-5766, 10.1029/96jc02775, 1997.

333   Millot, C., and Crepon, M.: Inertial oscillations on the continental-shelf of the Gulf of Lions -

334   observations and theory, Journal of Physical Oceanography, 11, 639-657, 10.1175/1520-

335   0485(1981)011<0639:iootcs>2.0.co;2, 1981.

336   Nicholls, J. F., Toumi, R., and Budgell, W. P.: Inertial currents in the Caspian Sea, Geophysical Research

337   Letters, 39, 10.1029/2012gl052989, 2012.

338   Pettigrew, N. R.: The dynamics and kinematics of the coastal boundary layer off Long Island, 1981.

339   Pollard, R. T., and Millard, R. C.: Comparison between ovserved and simulated wind-generated inertial

340   oscillations, Deep Sea Research, 813-821, 1970.

341   Price, J. F.: Upper ocean response to a hurricane, Journal of Physical Oceanography, 11, 153-175,
342   10.1175/1520-0485(1981)011<0153:uortah>2.0.co;2, 1981.

343   Shearman, R. K.: Observations of near-inertial current variability on the New England shelf, Journal of
344   Geophysical Research, 110, 10.1029/2004jc002341, 2005.

345   Sun, Z., Hu, J., Zheng, Q., and Li, C.: Strong near-inertial oscillations in geostrophic shear in the
346   northern South China Sea, Journal of Oceanography, 67, 377-384, 10.1007/s10872-011-0038-z, 2011.

347   Webster, F.: Observation of inertial period motions in the deep sea, Reviews of Geophysics, 6, 473-
348   490, 1968.

349   Xing, J. X., Davies, A. M., and Fraunie, P.: Model studies of near-inertial motion on the continental
350   shelf off northeast Spain: A three-dimensional two-dimensional one-dimensional model comparison
351   study, J Geophys Res-Oceans, 109, 10.1029/2003jc001822, 2004.

352   Zheng, Q., Lai, R. J., and Huang, N. E.: Observation of ocean current response to 1998 Hurricane
353   Georges in the Gulf of Mexico, Acta Oceanol. Sin., 25, 1-14, 2006.

354

355

356

357

358

359

360

361

362

363

364

365

366

367

368   **Figures**

369

370
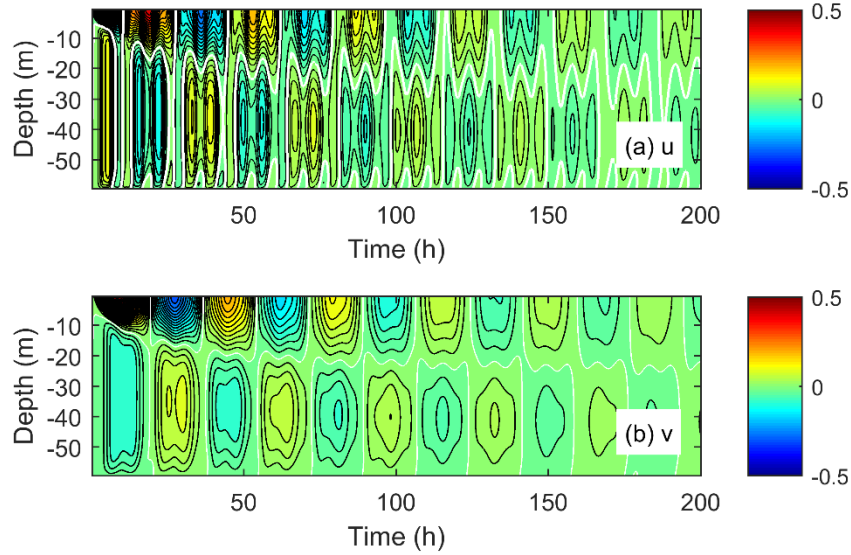
371   Fig. 1 Velocities (*u* and *v*, m/s) at x=70 km. The white lines denote the value of zero. The contour

372   interval is 0.02 m/s for both panels.

373

374
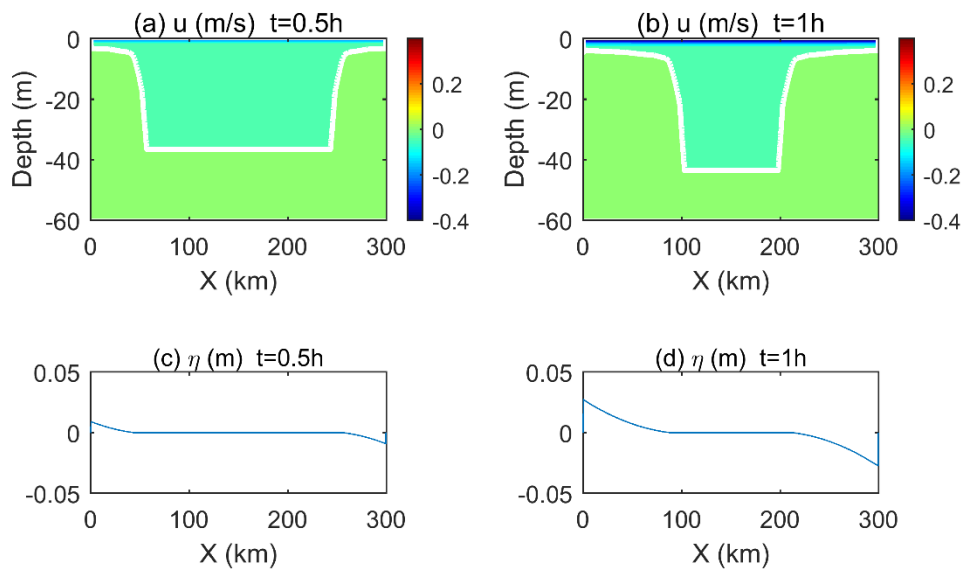
375   Fig. 2 Snapshots of eastward velocity and elevation (η) at t=0.5 and 1 hour. The white lines represent
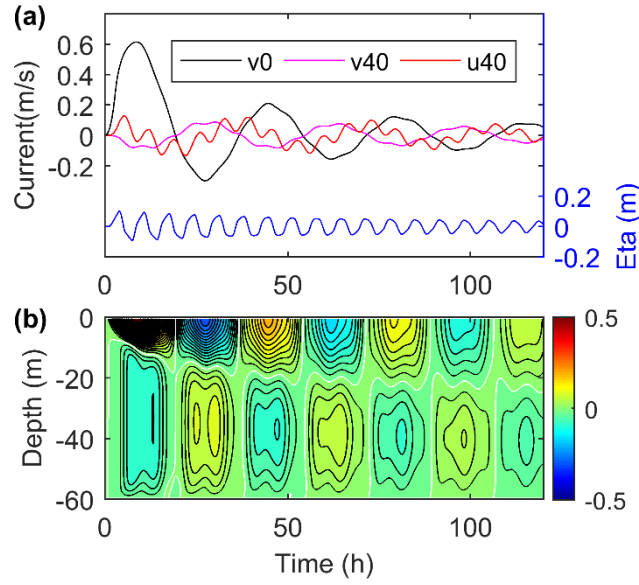
376   the value of zero.

14

377

Fig. 3 (a) Time series of velocities and elevation at x=100 km. 'v0' and 'v40' mean the northward

velocity (*v*) at depths of 0 m and 40 m, and 'u40' is the eastward velocity (*u*) at 40 m. (b) Contours of *v*

at x=100 km. The white lines denote the value of zero, and the contour interval is 0.02 m/s.

381

382
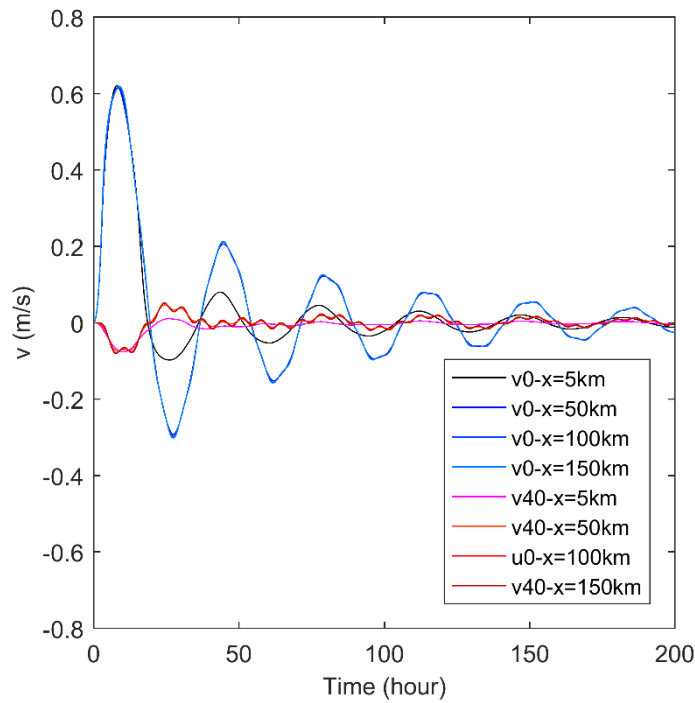
Fig. 4 Time series of the northward velocity (*v*) at different depths and positions. 'v0' and 'v40' mean *v*

at depths of 0 m and 40 m.

15

385

386
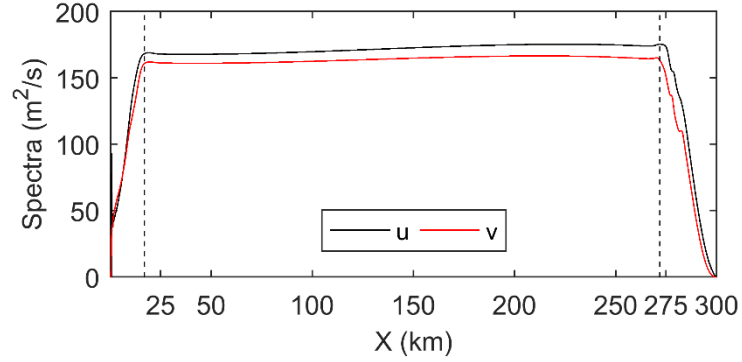
Fig. 5 Spatial variation of deph-mean spectra of velocities in near-inertial band for the homogeneous

case.

389

390
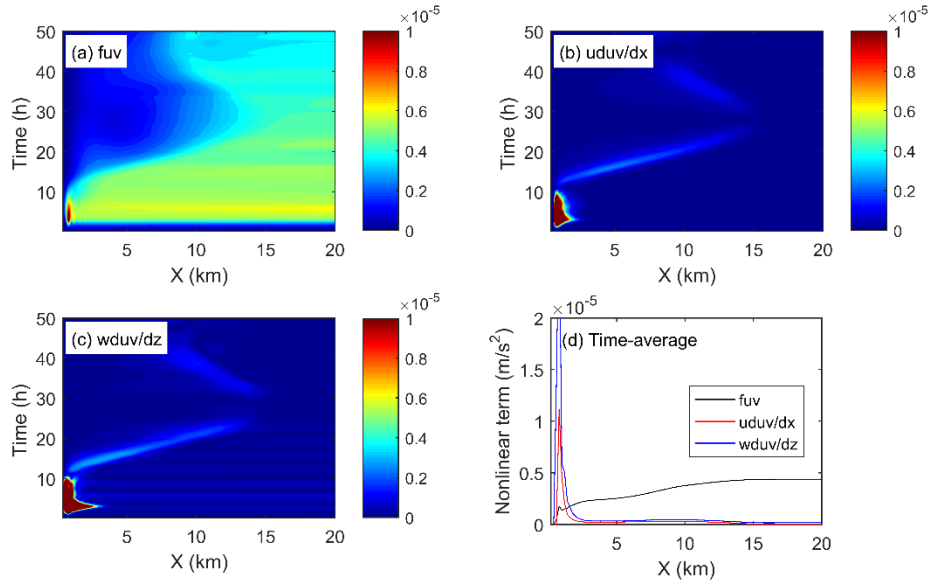
Fig 6. Variation of depth-mean inertial and nonlinear terms (m/s²). The inertial term (a) is calculated as

$\left| f(u+iv) \right|$, the horizontal nonlinear term (b) is $\left| u\left(\partial u / \partial x + i\partial v / \partial x \right) \right|$, and the vertical nonlinear

term (c) is $\left| w\left(\partial u / \partial z + i\partial v / \partial z \right) \right|$. (d) Time averaged value for the first 50 hours.

394

16

395
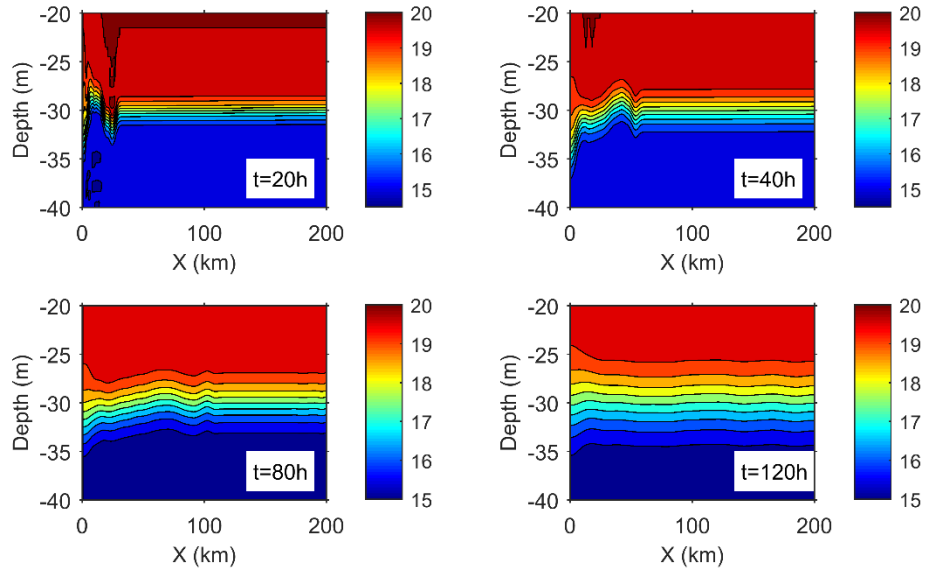
Fig. 7 Snapshots of temperature profiles at t=20h, 40h, 80h and 120h. The contour interval is 0.5 ℃.

397

398
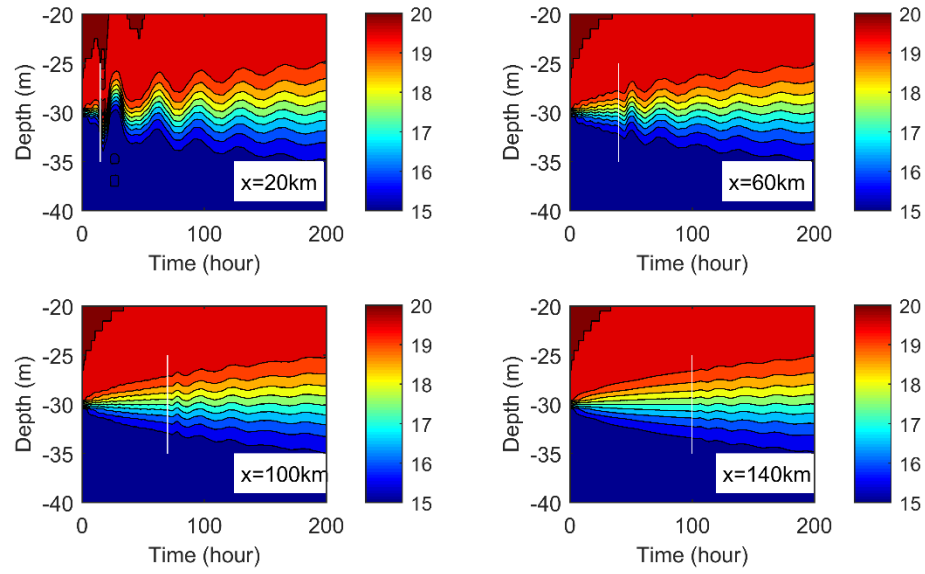
Fig. 8 Time series of temperature at x=20, 60, 100 and 140 km. White lines denote arrival of internal
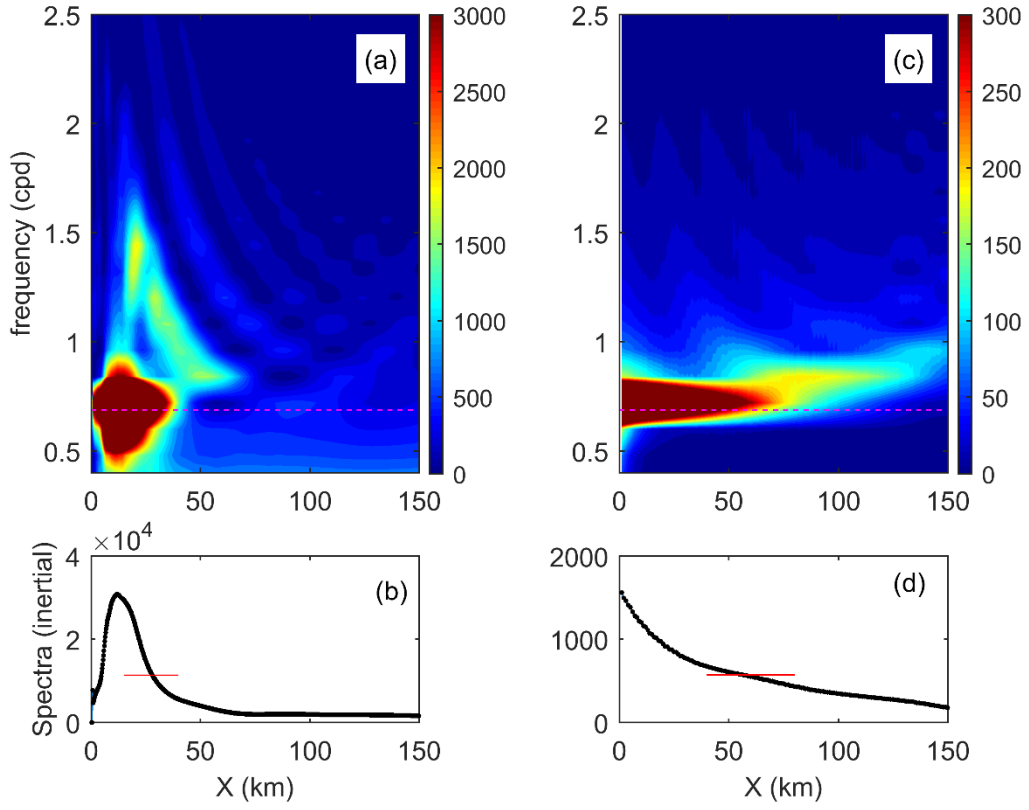
waves. The contour interval is 0.5 ℃.

401

402

Fig. 9 (a) Spectra of the temperature at the mid-depth (z=-30 m). The pink dash line represents the

inertial frequency. (b) Sum of spectra in inertial band with a red line denoting the e-folding value of the

peak. (c) Theoretical spectra of mid-depth elevation calculated from the solution in the form of a Bessel

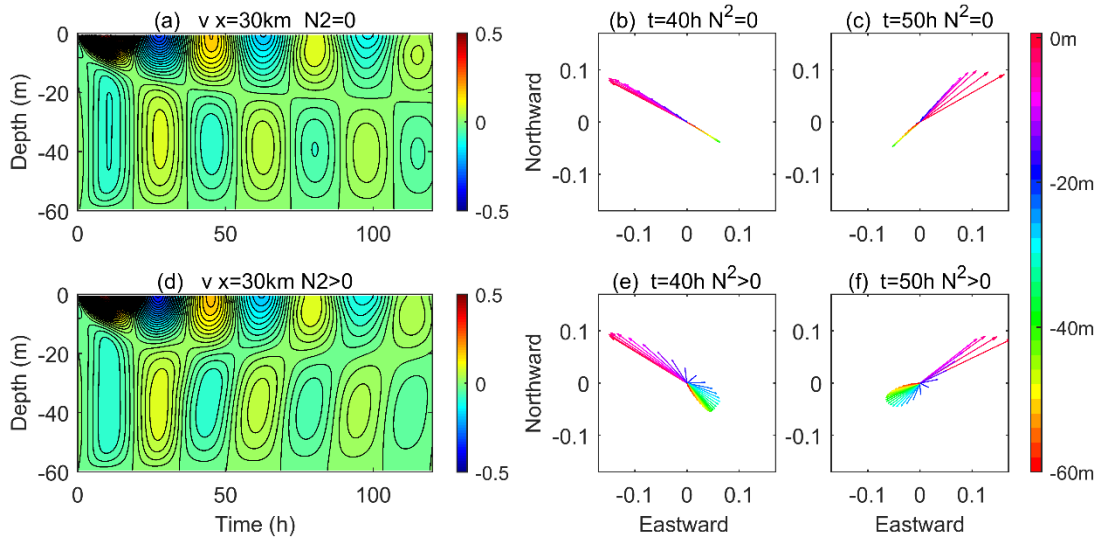function as in Eq. 3.16 of Pettigrew (1981). (d) Same as (b) but for theoretical spectra.

407

408

409   Fig. 10 Distribution of near-inertial currents (*v*, m/s) and current spirals for the cases without (a, b, c)

410   and with (d, e, f) stratification at x=30 km. The near-inertial currents are obtained by applying a band-

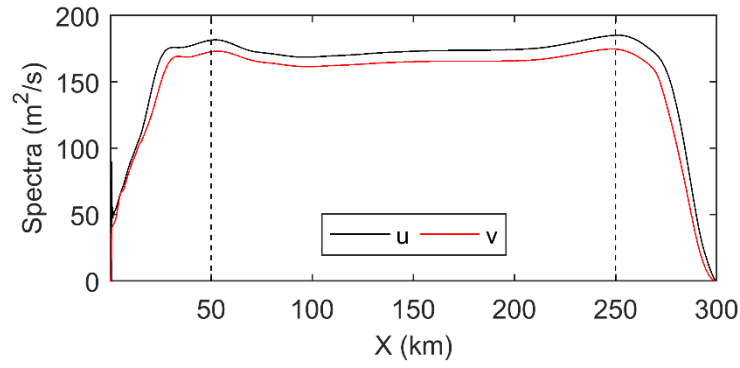411   pass filter. The contour interval is 0.02 m/s.

412

413

414   Fig. 11 Spatial variation of depth-mean spectra of velocities in near-inertial band for the stratified case.
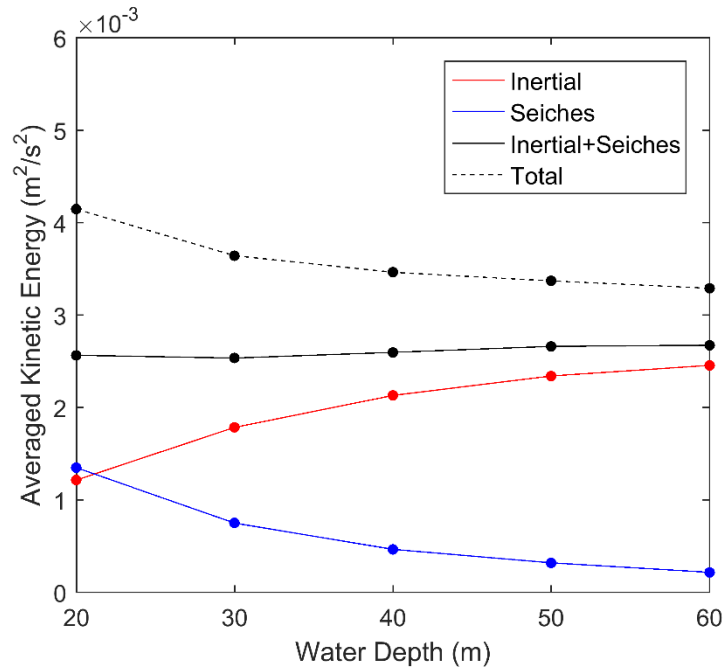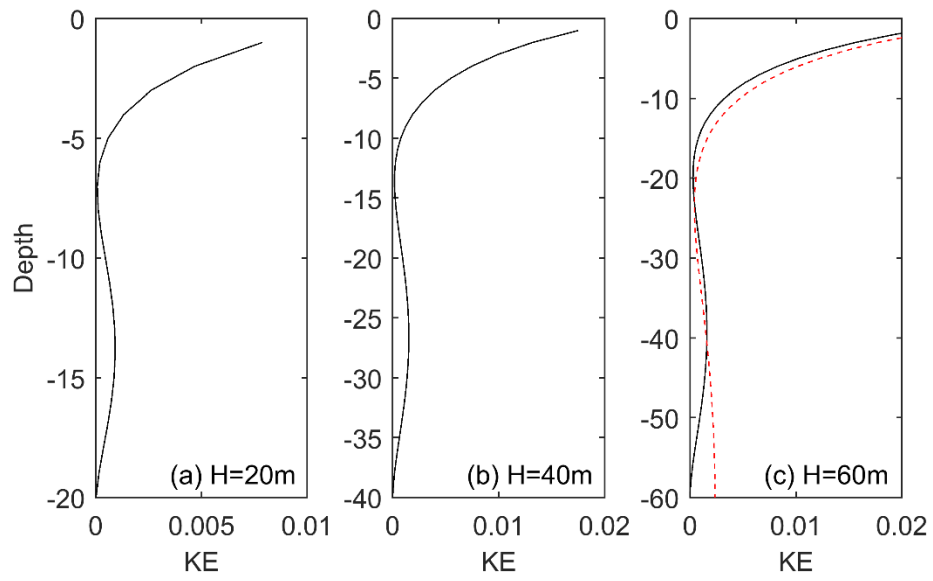
415

416

417   Fig. 12 The kinetic energy of near-inertial motions and seiches for different water depths. For each

418   case, the currents are ban-pass filtered to get currents for each type of motions which are then averaged

419   over time and integrated over space to obtain a final value.

19

420

421

422   Fig. 13 Vertical profile of averaged inertial kinetic energy for the homogeneous cases with water depths

423   of 20 m, 40 m and 60 m. The red dash line in (c) denotes the slip case.